Hindawi
Shock and Vibration
Volume 2018, Article ID 1056397, 14 pages
https://doi.org/10.1155/2018/1056397

Research Article

Transverse Vibration of Rotating Tapered Cantilever Beam with Hollow Circular Cross-Section

Zhongmin Wang and Rongrong Li

School of Civil Engineering and Architecture, Xi'an University of Technology, Xi'an 710048, China

Correspondence should be addressed to Zhongmin Wang; wangzhongm@xaut.edu.cn

Received 26 October 2017; Accepted 29 January 2018; Published 28 March 2018

Academic Editor: Matteo Filippi

Problems related to the transverse vibration of a rotating tapered cantilever beam with hollow circular cross-section are addressed, in which the inner radius of cross-section is constant and the outer radius changes linearly along the beam axis. First, considering the geometry parameters of the varying cross-sectional beam, rotary inertia, and the secondary coupling deformation term, the differential equation of motion for the transverse vibration of rotating tapered beam with solid and hollow circular cross-section is derived by Hamilton variational principle, which includes some complex variable coefficient terms. Next, dimensionless parameters and variables are introduced for the differential equation and boundary conditions, and the differential quadrature method (DQM) is employed to solve this differential equation with variable coefficients. Combining with discretization equations for the differential equation and boundary conditions, an eigen-equation of the system including some dimensionless parameters is formulated in implicit algebraic form, so it is easy to simulate the dynamical behaviors of rotating tapered beams. Finally, for rotating solid tapered beams, comparisons with previously reported results demonstrate that the results obtained by the present method are in close agreement; for rotating tapered hollow beams, the effects of the hub dimensionless angular speed, ratios of hub radius to beam length, the slenderness ratio, the ratio of inner radius to the root radius, and taper ratio of cross-section on the first three-order dimensionless natural frequencies are more further depicted.

1. Introduction

The dynamical problem of rotating uniform and nonuniform solid beam is widely used in many practical engineering, such as helicopter rotor blades and wind turbine blades. Also, the dynamics of rotating tapered hollow beams is of practical significant, for example, rotating tank gun barrel (hollow circular cross-section). As pointed out in [1], in dynamical analysis, a rotating beam differs from a nonrotating beam because it also possesses centrifugal stiffness and Coriolis effects that influence its dynamical characteristics. Besides the above effects, there are some complicated factors, including the secondary coupling deformation term, coupling effect, and the variable coefficient differential equation. Therefore, the methodologies and solutions for rotating nonuniform beam turn out to be cumbersome.

The dynamic analysis of rotating uniform beams has been the subject of many articles and received much attention. Yoo and Shin [2] investigated the effect of centrifugal force for rotating uniform cantilever beams and used a modal formulation to obtain the natural frequencies and mode shape. Tsai et al. [3] proposed the corotational finite element method combined with floating frame method to derive differential equation of motion for the rotating inclined Euler uniform beams at constant angular speed and investigated the steady-state deformation and the natural frequencies of infinitesimal free vibration. Vinod Kumar and Ganguli [4] used the static part of the homogeneous differential equation of violin strings to obtain new shape functions for the finite element analysis of rotating Timoshenko beams. Aksencer and Aydogdu [5] studied flapwise vibration of rotating composite beams, which are used in different beam theories, including Euler-Bernoulli, Timoshenko, and Reddy beam theories, and obtained some results for different orthotropy ratios, rotation speed, hub ratio, length to thickness ratio of the rotating composite beam, and different boundary conditions. Li et al. [6] developed a new dynamic model of a planar rotating hub-beam system, where the beam is of an Euler-Bernoulli type and the deformation of the beam is described by the slope angle and stretch strain of the centroid line of the beam. They obtained four corresponding spatially discretized models, that is, ESA, FOSA, SOSA, and SSOSA model, and calculated natural frequencies and mode shapes of the system with the chordwise bending and stretching coupling effect. J. W. Lee and J. Y. Lee [7] investigated the effects of cracks on the natural frequencies of a rotating Bernoulli-Euler beam using a new numerical method in which these effects can be computed simply using the transfer matrix method.

In recent years, more studies related to transverse vibration of rotating nonuniform beams can be found in the following papers. Gunda and Ganguli [8] developed new interpolating functions which satisfy the static part of the homogenous governing differential equation for rotating uniform and tapered beams and imposed as a constraint equation in the derivation of the shape functions. Cheng et al. [9] investigated vibration characteristics of cracked rotating tapered beam by p-version finite element method and analyzed the effects of crack location, crack size, rotating speed, and hub radius on vibration characteristics of the beam. Bulut [10] considered out-of-rotation plane bending vibrations of rotating composite beam with periodically varying speed and further examined the effect of taper ratio on dynamic stability of this parametrically system. Banerjee and Jackson [11] addressed the free vibration problem of a rotating tapered Rayleigh beam by developing its dynamic stiffness matrix. In their analysis, the effects of centrifugal stiffening, an outboard force, an arbitrary hub radius, and importantly, the rotary inertia (Rayleigh beam) are included. Sarkar and Ganguli [12] proposed an inverse problem approach for dynamics of the rotating nonuniform Euler-Bernoulli beam and showed that there exists a certain class of rotating Euler-Bernoulli beam, having cantilever and pinned-free boundary conditions, which has a closed-form polynomial solution to its governing differential equation. At the same year, they also studied the free vibration of a nonhomogeneous rotating Timoshenko beam, having uniform cross-section, using an inverse problem approach, for both cantilever and pinned-free boundary conditions [13]. Tang et al. [14] studied free vibration of rotating tapered cantilever beams with rotary inertia using the integral equation method and analyzed the effects of the rotary inertia, angular speed, taper ratio, and hub radius. Li and Zhang [15] developed a new rigid-flexible coupled dynamic model to study dynamics of rotating axially functionally graded (FG) tapered beams by using the B-spline method (BSM) and observed some new interesting phenomena of frequency veering and mode shift in a rotating axially FG tapered beam when the B-S coupling effect is included. Huo and Wang [16] derived the nonlinear dynamic equations of a rotating, double-tapered, cantilever Timoshenko beam and analyzed the effect of angular speed, hub radius, slenderness ratio, and the height and width taper ratios on the natural frequencies of the rotating Timoshenko beam when the rotation beam is in a steady state, in which the extensional deformation of the beam is considered. Panchore et al. [17, 18] investigated free vibration problem of a rotating Euler-Bernoulli beam and a rotating Timoshenko beam using meshless local Petrov-Galerkin method and introduced a locking-free shape function formulation with an improved radial basis function interpolation. Ghafarian and Ariaei [19] presented a new procedure for determining natural frequencies and mode shapes of a system of elastically connected multiple rotating tapered beams through a differential transform method, which obey the Timoshenko beam theory, and discussed the effects of the rotational speed, hub radius, taper ratios, rotary inertia, shear deformation, slenderness ratio, and elastic layer stiffness coefficients on the natural frequencies. Ghafari and Rezaeepazhand [20] presented free vibration analysis of rotating composite beams with arbitrary cross-section using dimensional reduction method. Adair and Jaeger [1] used the computational approach of AMDM to analyze the free vibration of nonuniform Euler-Bernoulli beams under various boundary conditions, rotation speeds, and hub radii and simultaneously obtained the natural frequencies and corresponding closed-form series solution of the mode shape. Panchore and Ganguli [21] studied the free vibration problem of a rotating Rayleigh beam using the quadratic B-spline finite element method. Other researchers also investigated the relevant second-order coupling term that represents longitudinal shrinking of the rotating beam caused by the transverse displacement. Li et al. [22] introduced a dynamic model of a rotating hub-functionally graded material beam system with the dynamic stiffening effect. In their work, the dynamic stiffening effect of the rotating hub-FGM beam system is captured by a second-order coupling term. Zhao and Wu [23] established the coupling equations of motion of a rotating three-dimensional cantilever beam to study the effects of Coriolis term and steady-state axial deformation on coupling vibration, which considered the longitudinal shrinkage caused by flapwise and chordwise bending displacement. At present, a large amount of articles relating to free vibration of rotating functionally graded plates or disk can be found (see, for instance, [24–26]).

In the above referenced articles, the model of rotating uniform beam and nonuniform beam have been considered, especially for rotating tapered beam, which has rectangular cross-section with linearly varying width and constant height, with linearly varying height and constant width, and with linearly varying width and height. However, to the best of the authors' knowledge, no research work related to the dynamics of a rotating beam with varying hollow circular cross-section (or rotating tapered hollow beam) has been yet presented. The dynamical of the system is of practical significant because rotating tapered hollow beams are widely used as structural components in the engineering field.

In this paper, the investigation proceeds as follows. First the geometry parameters of a rotating tapered cantilever beam with hollow circular cross-section are described, and the governing differential equation of motion for transverse free vibration of a rotating tapered Rayleigh beam is derived using Hamilton variational principle. Next, for harmonic oscillation, the differential equation with variable coefficients is solved using the differential quadrature method, and an eigen-equation of the system for dimensionless parameters is formulated in explicit algebraic form. Finally, for rotating solid tapered beams, comparisons with previously reported

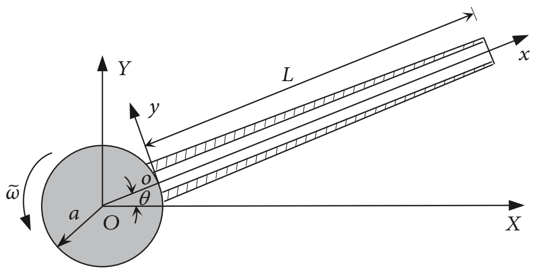

FIGURE 1: Schematic diagram of a rotating tapered cantilever beam with hollow circular cross-section.

results demonstrate that the results obtained by the present method are in close agreement; for rotating tapered hollow beams, the effects of the hub dimensionless angular speed, ratios of hub radius to beam length, the slenderness ratio, the ratio of inner radius to the root radius, and taper ratio of cross-section on the first three-order dimensionless natural frequencies are more further depicted.

2. Parameters of Rotating Tapered Cantilever Beam with Hollow Circular Cross-Section

Figure 1 shows the schematic diagram of a rotating tapered cantilever beam with hollow circular cross-section, which has length L, elastic modulus E, and density ρ and is fixed at point o of a rigid hub with radius a. The hub is rotating in the horizontal plane around point O with a rotating angular speed $\tilde{\omega}$. A fixed (inertial) planar coordinate system OXY through the fixed point O and a floating coordinate system oxy that is tangent to the attachment point of the beam to the hub are prescribed, respectively. The latter (oxy) relative to the former (OXY) rotates with a rotation angle θ of large range motion.

The rotating beam with varying hollow circular cross-section is considered, whose outer diameter varies linearly and the inner diameter keeps unchanged along its longitudinal x-axis, as shown in Figure 2. The beam has the root radius R_1 (at $x = 0$) and the end radius R_2 (at $x = L$), the wall thickness $e(x)$ versus the coordinate x, and the radius $R_p(x)$ at the middle line of the wall thickness for any cross-section. A local coordinate system with a normal direction n and tangential direction s at the central line of hollow circular cross-section is adopted.

The average radius $R_p(x)$ and the wall thickness $e(x)$ can be expressed, respectively, as follows:

$$R_p(x) = \frac{R_1}{2}\left[1 - (1-\lambda)\frac{x}{L}\right] + \frac{d}{4},$$
$$e(x) = R_1\left[1 - (1-\lambda)\frac{x}{L}\right] - \frac{d}{2} = 2R_p(x) - d, \tag{1}$$

where $\lambda = R_2/R_1$ is called the taper ratio of cross-section. It is also stipulated that the section size of the beam decreases and increases linearly from the root to the end, that is, $\lambda \in [d/2R_1, \infty]$, in which $d/2R_1$ is denoted by β (called the ratio of inner radius to the root radius). There are two particular cases: one is a uniform beam when $R_2 = R_1$, that is, $\lambda = 1$, and the other is a particular varying cross-section beam when $R_2 = d/2$, that is, $\lambda_{\min} = d/2R_1$.

The area of any cross-section and its moment of inertia with respect to axis z can be expressed, respectively, as

$$\begin{aligned} A_p(x) &= \pi\left(R_p + \frac{e}{2}\right)^2 - \pi\left(\frac{d}{2}\right)^2 \\ &= \pi R_1^2\left\{\left[1 - (1-\lambda)\frac{x}{L}\right]^2 - \beta^2\right\} = A_1 A_\lambda(x), \\ I(x) &= \frac{\pi}{64}\left[D^4(x) - d^4\right] = \frac{\pi}{64}\left[[2e(x)+d]^4 - d^4\right] \\ &= \pi R_p^{\,3}(x)\,e(x)\left[1 + \frac{e^2(x)}{4R_p^{\,2}(x)}\right] \\ &= \frac{\pi}{64}(2R_1)^4\left\{\left[1 - (1-\lambda)\frac{x}{L}\right]^4 - \beta^4\right\} \\ &= I_1 I_\lambda(x), \end{aligned} \tag{2}$$

where $A_1 = \pi R_1^2$ and $I_1 = (\pi/4)R_1^{\,4}$ are the area and the moment of inertia with respect to axis z of the root cross-section of the beam, respectively, $A_2 = (\pi/4)d^2$, $I_\lambda(x)$ and $A_\lambda(x)$ are given by

$$I_\lambda(x) = \left[1 - (1-\lambda)\frac{x}{L}\right]^4 - \beta^4,$$
$$A_\lambda(x) = \left[1 - (1-\lambda)\frac{x}{L}\right]^2 - \beta^2. \tag{3}$$

Any hollow circular cross-section of the beam is shown as Figure 3. The vertical coordinate of any point M can be expressed, respectively, as

$$y = y(s) + n\sin\alpha = y(s) - n\frac{\mathrm{d}z(s)}{\mathrm{d}s}. \tag{4}$$

3. Differential Equation of Motion

3.1. The Description of the Deformation Field. Figure 4 shows that $\mathbf{r}_a$ is a radius vector of the original point o of floating coordinate system oxy with respect to the point O of the inertial coordinate system OXY, $\mathbf{x}_p$ is a radius vector of any point P_0, which is on the axis of the beam before deformation, the point P is the positions of the point P_0 after deformation, and $\mathbf{u}_p$ is a displacement vector of the point P_0.

The vector of point P_0 relative to original point O of inertial coordinate system OXY can be expressed as

$$\mathbf{r}_p = \mathbf{r}_a + \mathbf{A}_\theta\left(\mathbf{x}_p + \mathbf{u}_p\right), \tag{5}$$

where

$$\mathbf{r}_a = \left[a\cos\theta \;\; a\sin\theta\right]^{\mathrm{T}},$$

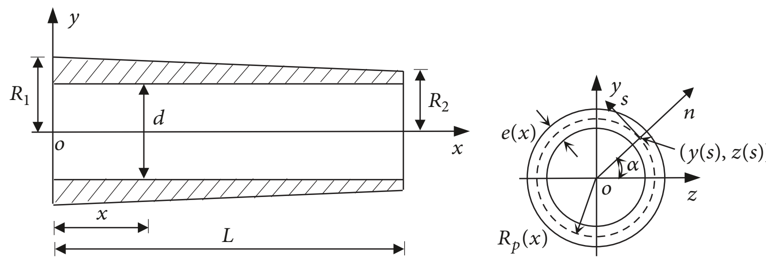

FIGURE 2: Geometry of rotating tapered cantilever beam with hollow circular cross-section and coordinate system.

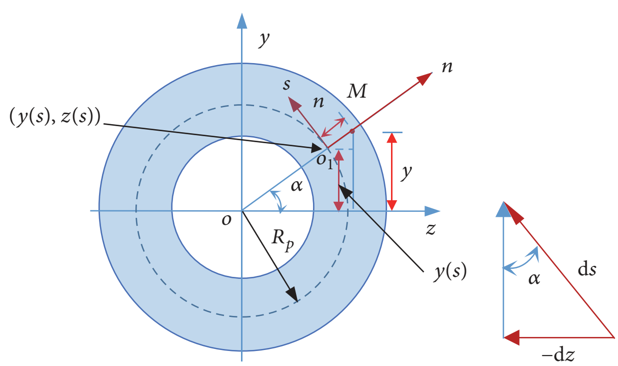

FIGURE 3: Any hollow circular cross-section of the beam and infinitesimal arc length.

$$\mathbf{x}_p = \begin{bmatrix} x & 0 \end{bmatrix}^{\mathrm{T}},$$

$$\mathbf{A}_\theta = \begin{bmatrix} \cos\theta & -\sin\theta \\ \sin\theta & \cos\theta \end{bmatrix} \text{ is a direction-cosine matrix of the floating base relative to the inertial base,}$$

$$\mathbf{u}_p = \begin{bmatrix} u_{px} \\ u_{py} \end{bmatrix} = \begin{bmatrix} u + u_c + u_b & w \end{bmatrix}^{\mathrm{T}} = \begin{bmatrix} u - \dfrac{1}{2}\displaystyle\int_0^x \left(w'\right)^2 \mathrm{d}x - yw' \\ w \end{bmatrix} \tag{6}$$

in which u and w are the axial displacement and the transverse bending deflection, respectively; $u_b = -yw' = -w'[y(s) - n(\mathrm{d}z(s)/\mathrm{d}s)]$ is axial displacement of any point caused by transverse bending, in which the prime denotes spatial derivatives with respect to x; $u_c = -(1/2)\int_0^x (w')^2 \mathrm{d}x$ is a second-order coupling term that represents longitudinal shrinking of the rotating tapered beam with hollow circular cross-section beam caused by the transverse displacement w. It includes the coupling effect between the axial displacement and transverse displacement of rotating tapered hollow beam.

Taking the derivative with respect to time for (4), the velocity vector of the point P_0 at the inertial coordinate system can be obtained

$$\dot{\mathbf{r}}_p = \dot{\mathbf{r}}_a + \dot{\boldsymbol{\theta}}\mathbf{A}_\theta\left(\mathbf{x}_p + \mathbf{u}_p\right) + \mathbf{A}_\theta\dot{\mathbf{u}}_p = \begin{bmatrix} -\dot{\theta}\left(a + x + u_c + u_b\right)\sin\theta - \dot{\theta}w\cos\theta + \left(\dot{u}_c + \dot{u}_b\right)\cos\theta - \dot{w}\sin\theta \\ \dot{\theta}\left(a + x + u_c + u_b\right)\cos\theta - \dot{\theta}w\sin\theta + \left(\dot{u}_c + \dot{u}_b\right)\sin\theta + \dot{w}\cos\theta \end{bmatrix}, \tag{7}$$

where $\dot{\boldsymbol{\theta}} = \begin{bmatrix} 0 & -\dot{\theta} \\ \dot{\theta} & 0 \end{bmatrix}$ is a antisymmetric matrix relating to angular speed $\dot{\theta}$, in which the over dot denotes derivative with respect to time t.

3.2. Differential Equation of Motion

3.2.1. Kinetic Energy of System. Kinetic energy of system consists of two parts: one is the kinetic energy of the hub

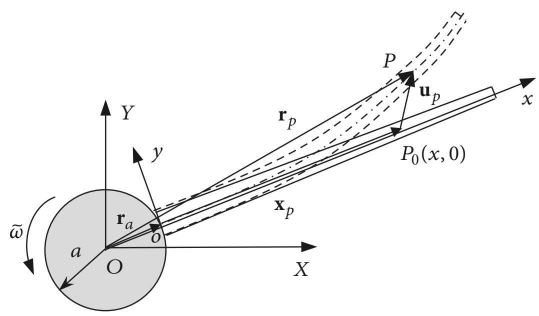

Figure 4: Schematic diagram of the deformation field.

and the other is the kinetic energy of the beam with hollow circular cross-section; namely,

$$T = T_H + T_P. \tag{8}$$

The kinetic energy of the hub is given by

$$T_H = \frac{1}{2} J_H \dot{\theta}^2, \tag{9}$$

where J_H is rotary inertia of the hub with respect to central axis.

Neglecting the axis displacement of the beam with hollow circular cross-section, the kinetic energy of the per unit length of the beam can be expressed as

$$\begin{aligned}\widetilde{T}_p &= \int_0^{2\pi R_p} \int_{-e/2}^{e/2} \frac{1}{2} \rho \left(\dot{\mathbf{r}}_p\right)^{\mathrm{T}} \dot{\mathbf{r}}_p \mathrm{d}n\, \mathrm{d}s = \frac{1}{2} m_c \left\{ \dot{w}^2 + \dot{u}_c{}^2 \right. \\ &+ \dot{\theta}^2 \left[w^2 + (a + x + u_c)^2 \right] \\ &\left. + 2\dot{\theta} \left[-\dot{u}_c w + \dot{w} (a + x + u_c) \right] \right\} \\ &+ \frac{1}{2} \left[\rho I_1 I_\lambda (x) \dot{\theta}^2 w_{,x}^2 + \rho I_1 I_\lambda (x) \dot{w}_{,x}^2 \right],\end{aligned} \tag{10}$$

where m_c is the effective mass of the per unit length of the beam; it can be expressed as

$$\begin{aligned}m_c &= \int_0^{2\pi R_p(x)} \rho e(x)\, \mathrm{d}s = \int_0^{2\pi R_p(x)} \rho e(x)\, \mathrm{d}s \\ &= \rho \cdot 2\pi R_p(x) e(x) = \rho A_p(x) = \rho A_1 A_\lambda (x).\end{aligned} \tag{11}$$

The kinetic energy of the beam with hollow circular cross-section can be rewritten as

$$\begin{aligned}T_P &= \int_0^L \widetilde{T}_p \mathrm{d}x = \frac{1}{2} \int_0^L m_c \left\{ \left(\dot{u}_c - \dot{\theta} w \right)^2 \right. \\ &\left. + \left[\dot{w} + \dot{\theta} (a + x + u_c) \right]^2 \right\} \mathrm{d}x = \frac{1}{2} \\ &\cdot \int_0^L \rho A_1 A_\lambda (x) \left\{ \dot{w}^2 + \dot{u}_c{}^2 \right. \\ &+ \dot{\theta}^2 \left[w^2 + (a + x + u_c)^2 \right] \\ &\left. + 2\dot{\theta} \left[-\dot{u}_c w + \dot{w} (a + x + u_c) \right]^2 \right\} \mathrm{d}x + \frac{1}{2} \\ &\cdot \int_0^L \rho I_1 I_\lambda (x) \left[\dot{\theta}^2 w_{,x}^2 + \dot{w}_{,x}^2 \right] \mathrm{d}x.\end{aligned} \tag{12}$$

Thus, substituting (9) and (12) into (8), the total kinetic energy of the system can be expressed as

$$\begin{aligned}T &= \frac{1}{2} J_H \dot{\theta}^2 + \frac{1}{2} \int_0^L \rho A_1 A_\lambda (x) \left\{ \dot{w}^2 + \dot{u}_c{}^2 \right. \\ &+ \dot{\theta}^2 \left[w^2 + (a + x + u_c)^2 \right] \\ &\left. + 2\dot{\theta} \left[-\dot{u}_c w + \dot{w} (a + x + u_c) \right]^2 \right\} \mathrm{d}x + \frac{1}{2} \\ &\cdot \int_0^L \rho I_1 I_\lambda (x) \left[\dot{\theta}^2 w_{,x}^2 + \dot{w}_{,x}^2 \right] \mathrm{d}x.\end{aligned} \tag{13}$$

3.2.2. Strain Energy of System. Neglecting the deformation energy caused by shear deformation, the strain energy of rotating beam with hollow circular cross-section is written as

$$V_\varepsilon = \int_V \frac{1}{2} \sigma_x \varepsilon_x \mathrm{d}V = \int_V \frac{1}{2} E \varepsilon_x^2 \mathrm{d}V, \tag{14}$$

where E is the elastic modulus of material; σ_x and ε_x represent the normal stress and normal strain in x direction, respectively.

In (6), ignoring the axial displacement and nonlinear term, the normal strain can be got by the relationship between strain and displacement: namely,

$$\varepsilon_x = \frac{\partial u_{px}}{\partial x} = -\left[y(s) - n \frac{\mathrm{d}z(s)}{\mathrm{d}s} \right] w''. \tag{15}$$

According to Figure 3, a geometrical relationship is given by

$$\frac{\mathrm{d}z(s)}{\mathrm{d}s} = -\sin\alpha = -\sin\left(\frac{s}{R_p} \right). \tag{16}$$

Thus, the strain energy of the beam with hollow circular cross-section can be rewritten as

$$\begin{aligned}V_\varepsilon &= \frac{1}{2} \int_0^L \int_{-e/2}^{e/2} \int_0^{2\pi} \varepsilon_x^2 \left(R_p(x) + n \right) \mathrm{d}\alpha\, \mathrm{d}s\, \mathrm{d}n = \frac{1}{2} \\ &\cdot \int_0^L \int_{-e/2}^{e/2} \int_0^{2\pi R_p} E \left[-\left[y(s) - n \frac{\mathrm{d}z(s)}{\mathrm{d}s} \right] w'' \right]^2 \\ &\cdot \left(\frac{R_p(x) + n}{R_p(x)} \right) \mathrm{d}s\, \mathrm{d}n\, \mathrm{d}x = \frac{1}{2} \int_0^L EI(x) \\ &\cdot \left(w'' \right)^2 \mathrm{d}x = \frac{1}{2} EI_1 \int_0^L I_\lambda (x) \left(w'' \right)^2 \mathrm{d}x.\end{aligned} \tag{17}$$

3.2.3. Derivation of Differential Equation of Motion. In this paper, Hamilton variational principle for elastic system is used to derive the differential equation of motion. The basis form of Hamilton variational principle can be showed as

$$\delta \int_{t_1}^{t_2} (T - V_\varepsilon)\,\mathrm{d}t = 0. \tag{18}$$

Substituting (13) and (17) into (18) and implementing a lot of variational operation and integration by parts, a variational expression is given by

$$\begin{aligned}&\int_0^L \Big\{-EI_1 I_\lambda(x) w'''' - 2EI_1 I_\lambda'(x) w''' - EI_1 I_\lambda''(x) w'' \\ &\quad + \rho A_1 A(x)\left[-\ddot{w} + \dot{\theta}^2 w - \ddot{\theta}(a + x + u_c) - 2\dot{\theta}\dot{u}_c\right] \\ &\quad + \rho I'(x)\dot{\theta}^2 w_{,x} + \rho I(x)\dot{\theta}^2 w_{,xx} - \rho I'(x)\ddot{w}_{,x} \\ &\quad - \rho I(x)\ddot{w}_{,xx}\Big\}\,\mathrm{d}x + \frac{\partial}{\partial x}\left[w' \int_x^L B(x,t)\,\mathrm{d}x\right] \\ &\quad = 0,\end{aligned} \tag{19}$$

where $B(x,t) = \rho A_1 A_\lambda(x)[-\ddot{u}_c + \dot{\theta}^2(a + x + u_c) + 2\dot{w}\dot{\theta} + \ddot{\theta}w]$.

Because second-order coupling deformation term u_c is a second-order small quantity, we can neglect some nonlinear terms and time-varying coupling terms in (19) to simplify the equation appropriately. Thus, the differential equation of motion of the rotating beam with hollow circular cross-section can be derived

$$\begin{aligned}&-EI_1 I_\lambda(x) w'''' - 2EI_1 I_\lambda'(x) w''' - EI_1 I_\lambda''(x) w'' \\ &\quad + \rho A_1 A_\lambda(x)\left[-\ddot{w} + \dot{\theta}^2 w - \ddot{\theta}(a + x) - \dot{\theta}^2 w'(a \right. \\ &\quad \left. + x) - 2\dot{w}\dot{\theta}w' - \ddot{\theta}ww'\right] + 2\dot{\theta}w'\dot{w}'\rho A_1\left[L - x \right. \\ &\quad \left. + \frac{(1-\lambda)^2}{3L^2}\left(L^3 - x^3\right) - \frac{(1-\lambda)}{L}\left(L^2 - x^2\right)\right] \\ &\quad - 2\dot{\theta}w'\dot{w}'\rho A_2(L - x) + \ddot{\theta}w'^2\rho A_1\left[L - x \right. \\ &\quad \left. + \frac{(1-\lambda)^2}{3L^2}\left(L^3 - x^3\right) - \frac{(1-\lambda)}{L}\left(L^2 - x^2\right)\right] \\ &\quad - \ddot{\theta}w'^2\rho A_2(L - x) + \rho A_1 w''\Big\{\left(2\dot{w}\dot{\theta} + \ddot{\theta}w + \dot{\theta}a\right) \\ &\quad \cdot\left[L - x + \frac{(1-\lambda)^2}{3L^2}\left(L^3 - x^3\right) \right. \\ &\quad \left. - \frac{(1-\lambda)}{L}\left(L^2 - x^2\right)\right] + \dot{\theta}^2\left[\frac{L^2 - x^2}{2} \right. \\ &\quad \left. + \frac{(1-\lambda)^2}{4L^2}\left(L^4 - x^4\right) - \frac{2(1-\lambda)}{3L}\left(L^3 - x^3\right)\right]\Big\} \\ &\quad - \rho A_2 w_{,xx}\left[\frac{\dot{\theta}^2}{2}\left(L^2 - x^2\right) + \left(2\dot{w}\dot{\theta} + \ddot{\theta}w + \dot{\theta}^2 a\right)(L \right. \\ &\quad \left. - x)\right] + \rho I'(x)\dot{\theta}^2 w' + \rho I(x)\dot{\theta}^2 w'' - \rho I'(x)\ddot{w}' \\ &\quad - \rho I(x)\ddot{w}'' = 0.\end{aligned} \tag{20}$$

Taking uniform rotation into consideration, that is, $\ddot{\theta} = 0$, $\dot{\theta} = \omega_0$, a differential equation of motion of the beam can be expressed as

$$\begin{aligned}&EI_1 I_\lambda(x) w'''' + 2EI_1 I_\lambda'(x) w''' + EI_1 I_\lambda''(x) w'' \\ &\quad + \rho A_1 A_\lambda(x)\ddot{w} - \rho I_1 I_\lambda(x)\ddot{w}'' - \rho I_1 I_\lambda'(x)\ddot{w}' \\ &\quad + \rho I_1 I_\lambda'(x)\omega_0{}^2 w' - \rho A_1 \omega_0{}^2(a\gamma_1 + \gamma_2) w'' \\ &\quad + \rho I_1 I_\lambda(x)\omega_0{}^2 w'' \\ &\quad + \rho A_1 \beta^2 \omega_0{}^2\left[a(L - x) + \frac{L^2 - x^2}{2}\right] w'' \\ &\quad + \rho A_1 A_\lambda(x)\omega_0{}^2(a + x) w' = 0\end{aligned} \tag{21}$$

in which $\lambda_1 = L - x + (1-\lambda)^2(L^3 - x^3)/3L^2 - (1-\lambda)(L^2 - x^2)/L$, $\lambda_2 = (L^2 - x^2)/2 + (1-\lambda)^2(L^4 - x^4)/4L^2 - (2(1-\lambda)/3L)(L^3 - x^3)$.

The boundary conditions of the cantilever beam are as follows:

$$\begin{aligned}x = 0:\quad & w = 0, \\ & w' = 0, \\ x = L:\quad & w'' = 0, \\ & E\frac{\mathrm{d}}{\mathrm{d}x}\left[I(x) w_{,xx}\right] - \rho I(x)\ddot{w}_{,x} + \rho I(x)\omega_0^2 w_{,x} \\ & = 0.\end{aligned} \tag{22}$$

3.3. Dimensionless Method of the Equation. For simplicity, the following dimensionless quantities are introduced: $\xi = x/L$, $\overline{w} = w/L$, $\tau = (t/L^2)\sqrt{EI_1/\rho A_1}$, $\omega = \omega_0 L^2\sqrt{\rho A_1/EI_1}$ (called dimensionless angular speed of the hub), $r_0 = a/L$ (called ratio of hub radius to beam length), and $r = \sqrt{I_1/A_1 L^2}$ (called slenderness ratio).

Dimensionless expression of (21) can be expressed as

$$\begin{aligned}&\frac{\partial^4 \overline{w}}{\partial \xi^4} + \frac{2I_\lambda'(\xi)}{I_\lambda(\xi)}\frac{\partial^3 \overline{w}}{\partial \xi^3} + \frac{I_\lambda''(\xi)}{I_\lambda(\xi)}\frac{\partial^2 \overline{w}}{\partial \xi^2} + \frac{A_\lambda(\xi)}{I_\lambda(\xi)}\frac{\partial^2 \overline{w}}{\partial \tau^2} \\ &\quad - \frac{I_\lambda'(\xi)}{I_\lambda(\xi)} r^2 \frac{\partial^3 \overline{w}}{\partial \tau^2 \partial \xi} - r^2 \frac{\partial^4 \overline{w}}{\partial \xi^2 \partial \tau^2} + \omega^2 r^2 \frac{\partial^2 \overline{w}}{\partial \xi^2}\end{aligned}$$

$$+\frac{I'_\lambda(\xi)}{I_\lambda(\xi)}\omega^2 r^2\frac{\partial\overline{w}}{\partial\xi}+\frac{A_\lambda(\xi)}{I_\lambda(\xi)}\omega^2(r_0+\xi)\frac{\partial\overline{w}}{\partial\xi}$$
$$-\frac{\omega^2}{I_\lambda(\xi)}(r_0\gamma_{11}+\gamma_{22})\frac{\partial^2\overline{w}}{\partial\xi^2}$$
$$+\frac{\beta^2\omega^2}{I_\lambda(\xi)}\left[r_0(1-\xi)+\frac{1-\xi^2}{2}\right]\frac{\partial^2\overline{w}}{\partial\xi^2}=0, \tag{23}$$

where $\gamma_{11} = (1-\xi)-(1-\lambda)(1-\xi^2)+((1-\lambda)^2/3)(1-\xi^3)$, $\gamma_{12} = (1-\xi^2)/2-(2(1-\lambda)/3)(1-\xi^3)+((1-\lambda)^2/4)(1-\xi^4)$.

Let the solution of (23) be $\overline{w}(\xi,\tau) = W(\xi)\exp(\Omega\tau)$; a differential equation of mode shape can be written as

$$\frac{d^4W}{d\xi^4}+\frac{2I'_\lambda(\xi)}{I_\lambda(\xi)}\frac{d^3W}{d\xi^3}+\frac{I''_\lambda(\xi)}{I_\lambda(\xi)}\frac{d^2W}{d\xi^2}+\Omega^2\frac{A_\lambda(\xi)}{I_\lambda(\xi)}W$$
$$-\frac{I'_\lambda(\xi)}{I_\lambda(\xi)}r^2\Omega^2\frac{dW}{d\xi}-r^2\Omega^2\frac{d^2W}{d\xi^2}+\omega^2r^2\frac{d^2W}{d\xi^2}$$
$$+\frac{I'_\lambda(\xi)\,\omega^2r^2}{I_\lambda(\xi)}\frac{dW}{d\xi}+\frac{A_\lambda(\xi)\,\omega^2}{I_\lambda(\xi)}(r_0+\xi)\frac{dW}{d\xi} \tag{24}$$
$$-\frac{\omega^2}{I_\lambda(\xi)}(r_0\gamma_{11}+\gamma_{22})\frac{d^2W}{d\xi^2}$$
$$+\frac{\omega^2\beta^2}{I_\lambda(\xi)}\left[r_0(1-\xi)+\frac{1-\xi^2}{2}\right]\frac{d^2W}{d\xi^2}=0,$$

where Ω is dimensionless natural frequency.

The dimensionless forms of the boundary conditions (22) are rewritten as

$$W(0)=0,$$
$$\frac{dW(0)}{d\xi}=0,$$
$$\frac{d^2W(1)}{d\xi^2}=0, \tag{25}$$
$$\frac{d^3W(1)}{d\xi^3}-r^2\left(\Omega^2-\omega^2\right)\frac{dW(1)}{d\xi}=0.$$

4. Differential Quadrature Method

In order to solve the differential equation with variable coefficients (24) and deal with the boundary conditions (25), the differential quadrature method (DQM) and the δ method are used, respectively. Selecting nonuniform nodes, the node coordinates are as follows [27, 28]:

$$X_1=0,$$
$$X_2=\delta,$$
$$X_{N-1}=1-\delta,$$
$$X_N=1,$$
$$X_i=\frac{1}{2}\left(1-\cos\frac{i-2}{N-3}\pi\right)\quad(i=3,4,\ldots,N-2), \tag{26}$$

where N is the numbers of nodes and δ is small parameter.

According to the DQM procedures, (24) can be discretized as follows:

$$\sum_{j=1}^{N}A_{ij}^{(4)}W_j+\frac{2I'_\lambda(\xi_i)}{I_\lambda(\xi_i)}\sum_{j=1}^{N}A_{ij}^{(3)}W_j+\frac{I''_\lambda(\xi_i)}{I_\lambda(\xi_i)}\sum_{j=1}^{N}A_{ij}^{(2)}W_j$$
$$+\Omega^2\frac{A_\lambda(\xi_i)}{I_\lambda(\xi_i)}W_i-\frac{I'_\lambda(\xi_i)}{I_\lambda(\xi_i)}r^2\Omega^2\sum_{j=1}^{N}A_{ij}^{(1)}W_j$$
$$-r^2\Omega^2\sum_{j=1}^{N}A_{ij}^{(2)}W_j+r^2\omega^2\sum_{j=1}^{N}A_{ij}^{(2)}W_j+\frac{I'_\lambda(\xi_i)}{I_\lambda(\xi_i)}$$
$$\cdot r^2\omega^2\sum_{j=1}^{N}A_{ij}^{(1)}W_j+\omega^2\frac{A_\lambda(\xi_i)}{I_\lambda(\xi_i)}(r_0+\xi_i)\sum_{j=1}^{N}A_{ij}^{(1)}W_j \tag{27}$$
$$-\frac{\omega^2}{I_\lambda(\xi_i)}\Bigg[(r_0\gamma_{11}+\gamma_{22})-\beta^2r_0(1-\xi_i)$$
$$-\beta^2\frac{1-\xi_i^2}{2}\Bigg]\sum_{j=1}^{N}A_{ij}^{(2)}W_j=0\quad(i=3,4,\ldots,N-2),$$

where $A_\lambda(\xi_i) = [1-(1-\lambda)\xi_i]^2-\beta^2$, $I_\lambda(\xi_i) = [1-(1-\lambda)\xi_i]^4-\beta^4$, $dI_\lambda(\xi_i)/d\xi = -4[1-(1-\lambda)\xi_i]^3(1-\lambda)$, $d^2I_\lambda(\xi_i)/d\xi^2 = 12[1-(1-\lambda)\xi_i]^2(1-\lambda)^2$.

The boundary conditions (25) can also be discretized as follows:

$$W_1=0, \tag{28a}$$
$$\sum_{j=1}^{N}A_{2j}^{(1)}W_j=0, \tag{28b}$$
$$\sum_{j=1}^{N}A_{N-1j}^{(2)}W_j=0, \tag{28c}$$
$$\sum_{j=1}^{N}A_{Nj}^{(3)}W_j-r^2\left(\Omega^2-\omega^2\right)\sum_{j=1}^{N}A_{Nj}^{(1)}W_j=0. \tag{28d}$$

Equations (27), (28a), (28b), (28c), and (28d) can be rewritten as a simpler matrix form

$$\left(\Omega^2\mathbf{M}+\Omega\mathbf{C}+\mathbf{K}\right)\mathbf{W}=0, \tag{29}$$

where $\mathbf{M}$, $\mathbf{C}$, and $\mathbf{K}$ are all $(N-2)\times(N-2)$ square matrix; $\mathbf{W}=\left[W_3\ \ W_4\ \ \cdots\ \ W_{n-2}\right]^{\mathrm{T}}$ is column matrix.

Equation (29) denotes a generalized eigenvalue problem. Based on the linear algebra theory, the sufficient and necessary conditions of homogeneous linear algebraic equations which create the nonzero solution are that the determinant of

Table 1: Comparison of the first three dimensionless natural frequencies of rotating solid tapered Euler-Bernoulli beams at $r_0 = 0$, $\beta = 0$, $r = 0$, $0 \leq \lambda \leq 1$.

ω	Ω	$\lambda = 1$		$\lambda = 0.75$		$\lambda = 0.5$		$\lambda = 0.25$		$\lambda = 0$
		Present	Ref. [14]	Present	Ref. [14]	Present	Ref. [14]	Present	Ref. [14]	Present
0	Ω_1	3.5164	3.5160	3.9570	3.9567	4.6257	4.6252	5.8293	5.8231	8.7445
	Ω_2	22.0366	22.0345	20.8091	20.807	19.5514	19.5476	18.5183	18.480	20.1042
	Ω_3	61.6960	61.6972	55.3500	55.3304	48.5953	48.5789	41.4611	41.321	36.5279
5	Ω_1	6.4499	6.4495	6.7732	6.7729	7.2905	7.2901	8.2653	8.2620	10.6634
	Ω_2	25.4483	25.4461	24.0673	24.0660	22.6379	22.6360	21.4209	21.384	22.8601
	Ω_3	65.2118	65.2050	58.6518	58.6364	51.7012	51.6918	44.4176	44.269	41.0619
10	Ω_1	11.2029	11.2023	11.4859	11.4856	11.9419	11.9415	12.7928	12.791	14.7477
	Ω_2	33.6417	33.6404	31.8863	31.8895	30.0289	30.0299	28.3381	28.301	29.4213
	Ω_3	74.6671	74.6493	67.5293	67.5316	60.0369	60.0399	52.2738	52.100	51.2478
15	Ω_1	16.1445	-	16.4165	-	16.8587	-	17.6745	-	19.4476
	Ω_2	43.9323	-	41.7005	-	39.2756	-	36.9308	-	37.5106
	Ω_3	87.9543	-	80.0153	-	71.7371	-	63.1548	-	59.9363

coefficients equals zero; thus, one can arrive to the following generalized eigen-equation:

$$\left|\Omega^2\mathbf{M} + \Omega\mathbf{C} + \mathbf{K}\right| = 0, \tag{30}$$

where the square matrices $\mathbf{M}$, $\mathbf{C}$, and $\mathbf{K}$ involve some parameters, such as ratios of hub radius to beam length, the slenderness ratio, the ratio of inner radius to the root radius, and taper ratio of cross-section, each dimensionless natural frequencies, and dimensionless angular speed of the hub.

5. Numerical Results and Analyses

5.1. Rotating Tapered Cantilever Beam with Solid Circular Cross-Section. In this paragraph, setting $\beta = 0$ in (24), we can obtain the differential equation of motion for rotating tapered beam with solid circular cross-section, where taper ratio $\lambda \in [0, \infty)$ is defined. It becomes evident that if the taper ratio $\lambda = 0$ and $\lambda = 1$, they are varying solid circular cross-section beam with zero radius at free end and entirely uniform solid circular cross-section, respectively. Prior to the presentation of our numerical results, let us first consider three particular cases to confirm the effectiveness of the present approach: a simple uniform nonrotating cantilever beam, a rotating tapered Euler-Bernoulli cantilever beam, and a rotating tapered Rayleigh cantilever beam, which is given by setting parameters $\omega = 0$, $r_0 = 0$, $r = 0$, and $\lambda = 1$, parameters $r_0 = 0$, $r = 0$, and parameters $r_0 = 0$, $1/r = 30$, respectively. In three cases, we calculate the first three-order dimensionless natural frequencies by selecting $N = 12$ for different taper ratio of cross-section and dimensionless angular speed, and some numerical results are tabulated in Tables 1 and 2 ($0 \leq \lambda \leq 1$). From the two tables, we can see that the numerical results in the present coincide well with the existing ones [14]. These verify that the method presented in this paper is efficient and accurate. The first three dimensionless mode shapes are shown as Figure 5 for $\omega = 10$, $\lambda = 1$, $r_0 = 0$, $\beta = 0$, and $r = 0$.

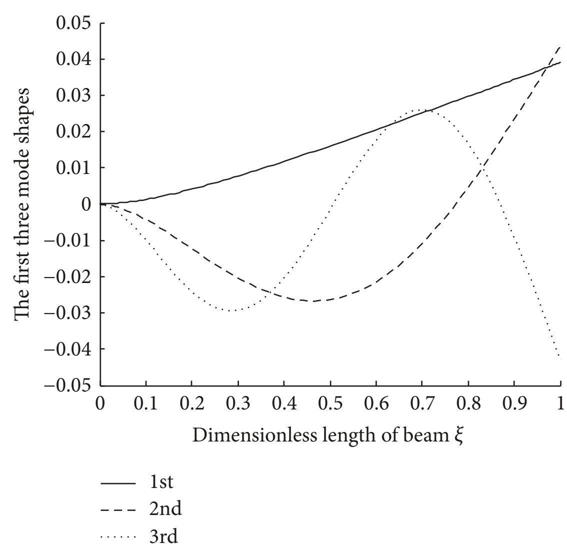

Figure 5: The first three dimensionless mode shapes for $\omega = 10$, $\lambda = 1$, $r_0 = 0$, $\beta = 0$, and $r = 0$.

Furthermore, in the case of $\lambda > 1$, for example, $1.25 \leq \lambda \leq 3.00$, that is, the radius of beam cross-section at free end is more than one at the cantilevered end, the first three-order dimensionless natural frequencies of a rotating tapered Rayleigh cantilever solid beam for three dimensionless angular speeds are tabulated in Table 3. It can be seen in Table 3 that as a whole, the first three-order dimensionless natural frequencies increase with the increase of dimensionless angular speeds.

Figure 6 shows the variation of the first three-order dimensionless natural frequencies of rotating tapered solid beams with dimensionless angular speed of the hub for three different ratios of hub radius to beam length $r_0 = 0, 0.5, 1$ at $\lambda = 0.5$, $r = 1/30$. It can be found from Figure 6 that, with the increase of the ratios of hub radius to beam length, the first three-order dimensionless natural frequencies increase. Figure 7 shows the variation of the first

Table 2: Comparison of the first three dimensionless natural frequencies of rotating solid tapered Rayleigh beams for different λ $(0 \le \lambda \le 1)$ at $r_0 = 0$, $\beta = 0$, $1/r = 30$.

ω	Ω	$\lambda = 1$		$\lambda = 0.75$		$\lambda = 0.5$		$\lambda = 0.25$		$\lambda = 0$
		Present	Ref. [14]	Present	Ref. [14]	Present	Ref. [14]	Present	Ref. [14]	Present
0	Ω_1	3.5073	3.5070	3.9486	3.9483	4.6174	4.6168	5.8198	5.8136	8.7267
	Ω_2	21.6497	21.6477	20.5498	20.5475	19.3883	19.3846	18.4214	18.3834	20.0372
	Ω_3	59.2069	59.2073	53.7093	53.6911	47.6173	47.6021	40.9588	40.825	36.5169
5	Ω_1	6.4254	6.4251	6.7524	6.7521	7.2720	7.2717	8.2469	8.2436	10.6360
	Ω_2	24.9759	24.9737	23.7510	23.7497	22.4394	22.4375	21.3029	21.266	22.7786
	Ω_3	62.5464	663.5392	56.8916	56.8774	50.6483	50.6397	43.8720	43.730	41.0472
10	Ω_1	11.1604	11.1598	11.4494	11.4490	11.9087	11.9083	12.7584	12.767	14.6997
	Ω_2	32.9667	32.9654	31.4395	31.4425	29.7515	29.7521	28.1722	28.136	29.3002
	Ω_3	71.5142	71.4977	65.4444	65.4472	58.7850	58.7878	51.6155	51.450	50.5772
15	Ω_1	16.0851	-	16.3650	-	16.8105	-	17.6223	-	19.3744
	Ω_2	43.0010	-	41.0951	-	38.9051	-	36.7064	-	37.3335
	Ω_3	84.0806	-	77.4631	-	70.2081	-	62.3423	-	59.2553

Table 3: The first three dimensionless natural frequencies of rotating solid tapered Rayleigh beams for different λ $(1.25 \le \lambda \le 3)$ at $r_0 = 0$, $\beta = 0$, $1/r = 30$.

ω	Ω	$\lambda = 1.25$	$\lambda = 1.50$	$\lambda = 1.75$	$\lambda = 2.00$	$\lambda = 2.25$	$\lambda = 2.5$	$\lambda = 2.75$	$\lambda = 3.00$
0	Ω_1	3.1877	2.9421	2.7461	2.5882	2.4704	2.4129	2.4613	2.6858
	Ω_2	22.6579	23.5718	24.3952	25.1281	25.7580	26.2480	26.5270	26.4787
	Ω_3	64.2417	68.9100	73.2615	77.3249	81.1317	84.7333	88.2071	91.6568
5	Ω_1	6.1987	6.0331	5.9156	5.8549	5.8827	6.0577	6.4683	7.2429
	Ω_2	26.0836	27.0745	27.9483	28.6698	29.2062	29.4743	29.3543	28.6666
	Ω_3	67.7177	72.5014	76.9672	81.1744	85.1868	89.0823	92.9551	96.9133
10	Ω_1	10.9632	10.8352	10.7906	10.8785	11.1850	11.8383	13.0323	15.1307
	Ω_2	34.3001	35.4363	36.3539	36.9976	37.2721	37.0347	36.0682	33.9720
	Ω_3	77.0509	82.1465	86.9066	91.4446	95.8797	100.3326	104.9216	109.7575
15	Ω_1	15.9065	15.8297	15.9030	16.2187	16.9153	18.1923	20.3830	24.3670
	Ω_2	44.5894	45.8474	46.7372	47.1832	47.0645	46.1947	44.2444	40.3254
	Ω_3	90.1006	95.6133	100.7463	105.6461	110.4616	115.3326	120.3820	125.7134

three-order dimensionless natural frequencies of rotating tapered solid beams with dimensionless angular speed of the hub for three different slenderness ratios $r = 1/30, 1/10$ at $\lambda = 0.5$, $r_0 = 0$. It can be seen from Figure 7 that, for two different $r = 1/30, 1/10$, the increase of slenderness ratio has scarce influence on the first-order dimensionless natural frequencies; however, it has significant influence on the second- and the third-order dimensionless natural frequency. This shows that the increase of rotary inertia makes the system natural frequency decrease, and this conclusion is consistent with those given by Timoshenko beam. Figure 8 shows the variation of the first three-order dimensionless natural frequencies of rotating tapered solid beams with dimensionless angular speed of the hub for three different taper ratios of cross-section $\lambda = 0.25, 0.5, 0.75$ at $r_0 = 0$, $r = 1/30$. It can be seen from Figure 8 that, with the increase of taper ratio, the first three-order dimensionless natural frequencies of the system decrease. It is noted that the increase of taper ratio has scarce influence on the first-order dimensionless natural frequency, it has slight influence on the second-order dimensionless natural frequency, and it has obviously an effect on the third-order dimensionless natural frequency. It should be pointed out that, as shown in Figures 6–8, in the case of the given ratios of hub radius to beam length, the slenderness ratio, and taper ratio of cross-section, the first three dimensionless natural frequencies of rotating tapered solid beam monotonically increase with dimensionless angular speed of the hub.

5.2. Rotating Tapered Cantilever Beam with Hollow Circular Cross-Section. For a rotating tapered cantilever beam with hollow circular cross-section, its inner diameter $d \ne 0$, that is, $\beta \ne 0$, and the taper ratio $\lambda \in [\beta, \infty)$ is defined. When $\lambda = \beta$, the outer radius of beam at free end is the same as its inner radius. When $\lambda = 1$, the beam is entirely uniform hollow circular cross-section. This section will mainly discuss the effect of ratios of hub radius to beam length, the slenderness ratio, the ratio of inner radius to the root radius, and taper ratio of cross-section on the first three dimensionless natural frequencies of rotating tapered hollow beams.

As a particular case of hollow circular cross-section, Table 4 gives the variation of the first three dimensionless

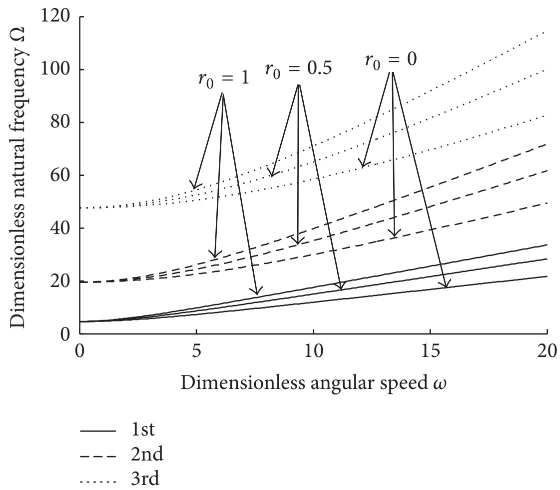

Figure 6: Variation of the first three dimensionless natural frequencies of rotating solid tapered beams with dimensionless angular speed of the hub for various $r_0 = 0, 0.5, 1$ at $\lambda = 0.5$, $r = 1/30$.

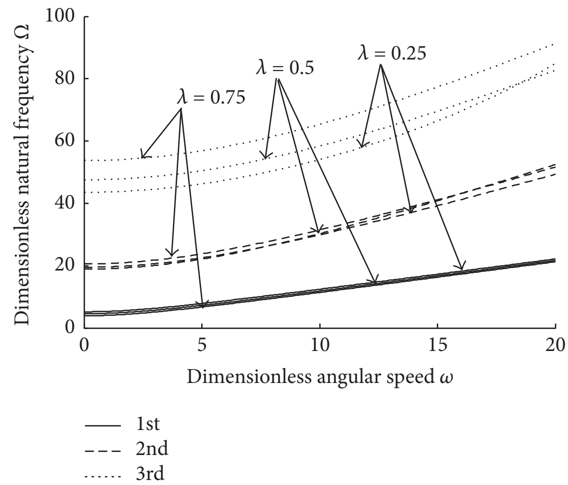

Figure 8: Variation of the first three dimensionless natural frequencies of rotating solid tapered beams with dimensionless angular speed of the hub for various $\lambda = 0.25, 0.5, 0.75$ at $r = 1/30$, $r_0 = 0$.

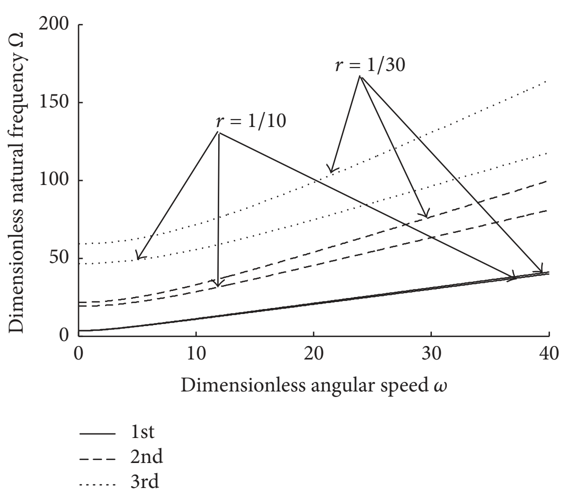

Figure 7: Variation of the first three dimensionless natural frequencies of rotating solid tapered beams with dimensionless angular speed of the hub for various $r = 1/30, 1/10$ at $\lambda = 0.5$, $r_0 = 0$.

natural frequencies of rotating uniform thin-wall cross-section beams with dimensionless angular speed of the hub for three different slenderness ratios $r = 0, 1/30, 1/10$ at $r_0 = 0$, $\beta = 0.92$, and $\lambda = 1$. It should be pointed out that the first three dimensionless natural frequencies of nonrotating beam in Table 4 equal the first three dimensionless natural frequencies 3.5156, 22.0336, and 61.7010 [29] of cantilever beam multiplied by $\sqrt{1+\beta^2}$. We can see that the numerical results in the present coincide well with the existing ones [29]. The first three dimensionless natural frequencies of the rotating uniform thin-wall cross-section beam decreased as the slenderness ratio was raised.

5.2.1. Effect of the Hub Dimensionless Angular Speed and Taper Ratio of Cross-Section. Table 5 gives the variation of the first three dimensionless natural frequencies of rotating tapered hollow beams with dimensionless angular speed of the hub for two different slenderness ratios $r = 1/30, 1/10$ and three ratios of inner radius to the root radius $\beta = 0.2, 0.4, 0.6$ at $\lambda = 0.75$. With this table, it is obvious that the first three dimensionless natural frequencies increase with the ratio of inner radius to the root radius, except the second-order dimensionless natural frequencies at $r = 1/10$, $\omega = 15$.

Figure 9 plots the curves between the first three-order dimensionless natural frequencies of rotating tapered hollow beam and dimensionless angular speed of the hub for $\lambda = 0.5, 0.75$ and $r = 1/30, 1/10$ at $\lambda = 0.5$, $r_0 = 0$, $\beta = 0.2$. With this figure, it is also understood that the first three-order dimensionless natural frequencies of rotating tapered hollow beam monotonically increase with dimensionless angular speed of the hub. Meanwhile, it is further noted in Figure 9(a) that, with the increase of the taper ratio of cross-section, the first-order dimensionless natural frequency of the system is reduced slightly. However, in Figures 9(b) and 9(c), with the increase of the taper ratio of cross-section, the values of the second- and third-order dimensionless natural frequencies of the system are increased.

In addition, it is also observed in Figure 9 that the increase of slenderness ratio makes three dimensionless natural frequencies of the system decrease, contrasting Figures 9(a), 9(b), and 9(c), obviously, and the effect of the slenderness ratio on the second- and third-order dimensionless natural frequencies is relatively greater than the first-order dimensionless natural frequency.

5.2.2. Effect of Ratios of Hub Radius to Beam Length and Slenderness Ratio. As it was expected in Table 6, the change of ratios of hub radius to beam length has no effect on the natural frequencies of nonrotating tapered beam ($\omega = 0$). It is also observed in Table 6 that, for rotating tapered beam, the dimensionless natural frequencies of the system increase with ratios of hub radius to beam length.

Figure 10 plots the curves between the first three-order dimensionless natural frequencies of rotating tapered

Table 4: The first three order dimensionless natural frequencies of rotating circular thin-wall cross-section beams at $r_0 = 0$, $\beta = 0.92$, $\lambda = 1$.

ω	Ω	$r = 0$ Present	$r = 0$ Ref. [29]	$r = 1/30$	$r = 1/10$
0	Ω_1	4.7781	4.7771	4.7555	4.5844
	Ω_2	29.9438	29.9393	28.9935	23.6666
	Ω_3	83.8339	83.8393	77.8914	54.3817
5	Ω_1	7.2326	-	7.1843	6.8112
	Ω_2	32.5368	-	31.4682	25.4442
	Ω_3	86.4579	-	80.2848	55.9058
10	Ω_1	11.7433	-	11.6598	10.9967
	Ω_2	39.2955	-	37.9215	30.0678
	Ω_3	93.8425	-	87.0105	60.1779
15	Ω_1	16.6095	-	16.4939	15.5592
	Ω_2	48.4647	-	46.6776	36.2668
	Ω_3	104.8728	-	97.0268	66.4979

Table 5: The first three order dimensionless natural frequencies of rotating tapered hollow beams for various ratio of inner radius to the root radius β ($r_0 = 0, \lambda = 0.75$).

ω	Ω	$r = 1/30$			$r = 1/10$		
		$\beta = 0.2$	$\beta = 0.4$	$\beta = 0.6$	$\beta = 0.2$	$\beta = 0.4$	$\beta = 0.6$
0	Ω_1	4.0743	4.4869	5.4689	4.0021	4.3928	5.3165
	Ω_2	21.1137	22.8085	25.9958	19.1933	20.4539	22.8066
	Ω_3	55.0759	59.0308	65.6330	45.1361	47.2503	50.6619
5	Ω_1	6.8283	7.0878	7.7613	6.6530	6.8756	7.4647
	Ω_2	24.2176	25.6314	28.3193	21.8856	22.8463	24.6981
	Ω_3	58.1504	61.7981	67.8694	47.5230	49.3294	52.2535
10	Ω_1	11.5023	11.6837	12.1584	11.1927	11.3104	11.6424
	Ω_2	31.7436	32.6600	34.3608	28.4415	28.8297	29.6427
	Ω_3	66.4593	69.3894	74.1474	53.9527	55.0169	56.7149
15	Ω_1	16.4109	16.5675	16.9725	15.9740	16.0415	16.2467
	Ω_2	41.2695	41.7660	42.5327	36.7455	36.5930	36.3560
	Ω_3	78.2143	80.3361	83.4935	62.9728	63.1570	63.3260

hollow beam and dimensionless angular speed of the hub for $r_0 = 0, 0.5, 1$ at $r = 1/30$, $\lambda = 0.5$. With this figure, the first three-order dimensionless natural frequencies of the system increase with dimensionless angular speed of the hub and ratios of hub radius to beam length.

Figure 11 plots the curves of the first three-order dimensionless natural frequencies with ratios of hub radius to beam length for two different taper ratios of cross-section $\lambda = 0.5$, 0.75 at $\omega = 5$, $r = 1/30$, $\beta = 0.3$. Figure 12 plots the curves of the first three-order dimensionless natural frequencies with ratios of hub radius to beam length for two different slenderness ratios $r = 1/30, 1/10$ at $\omega = 5$, $\lambda = 0.5$, $\beta = 0.3$. It can be seen in Figures 11 and 12 that, for different taper ratio of the cross-section and slenderness ratios, with the increase of ratios of hub radius to beam length, the first three-order dimensionless natural frequencies of the system are almost linearly increased. Meanwhile, it is noted that the influence of the slenderness ratio on the third-order natural frequency of the system is more obvious than that of the first order and the second order.

6. Conclusion

In this paper, a new type of transverse vibration of a rotating tapered cantilever beam with linearly varying solid and hollow circular cross-section, that is, rotating tapered beam, was presented. The rotating beam, which is considered a tapered cantilever beam, is modeled by the Rayleigh beam theory. Considering the secondary coupling deformation term, the differential equation of motion for the transverse vibration of rotating tapered beam with solid and hollow circular cross-section is derived by Hamilton variational principle, which includes some complex variable coefficient terms. A differential quadrature method to solve the above-mentioned differential equation with variable coefficients was employed to simulate the dynamical behaviors of tapered rotating beams. Also, for two types of rotating tapered beams with solid and hollow circular cross-section, the effects of the hub dimensionless angular speed, ratios of hub radius to beam length, the slenderness ratio, the ratio of inner radius to the root radius, and taper ratio of cross-section on the first three-order dimensionless natural frequencies are

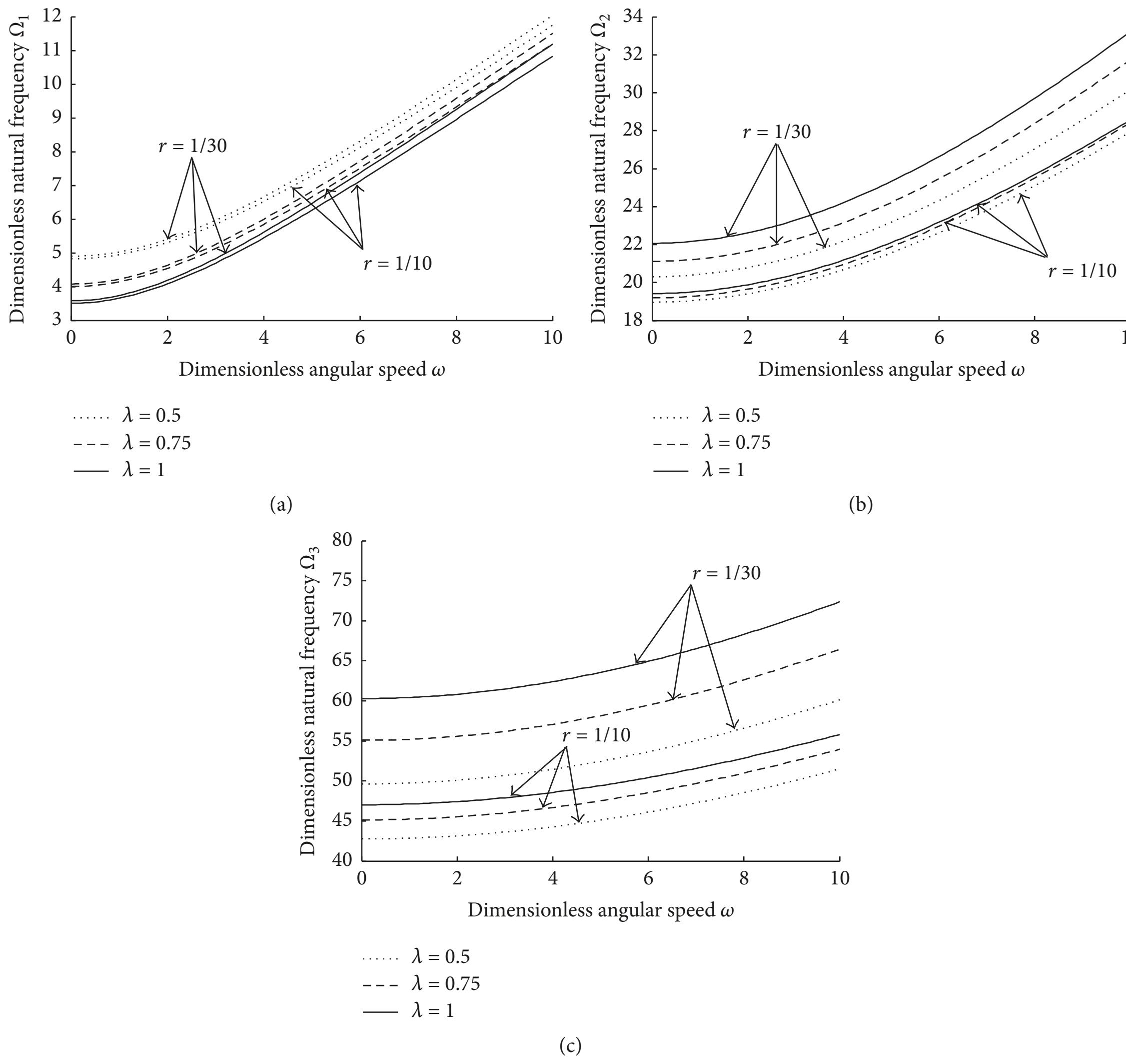

FIGURE 9: Variation of the first three dimensionless natural frequencies of rotating tapered hollow beam with dimensionless angular speed of the hub for different values of $\lambda = 0.5$, 0.75 and $r = 1/30$, 1/10 at $r_0 = 0$, $\beta = 0.2$: (a) 1st mode; (b) 2nd mode; and (c) 3rd mode.

TABLE 6: The first three-order dimensionless natural frequencies of rotating tapered hollow beams for various ratios of hub radius to beam length r_0 ($\beta = 0.2$).

ω	Ω	$r = 1/10$			$r = 1/30$		
		$r_0 = 0.1$	$r_0 = 0.5$	$r_0 = 1$	$r_0 = 0.1$	$r_0 = 0.5$	$r_0 = 1$
0	Ω_1	4.0021	4.0021	4.0021	4.0743	4.0743	4.0743
	Ω_2	19.1933	19.1933	19.1933	21.1137	21.1137	21.1137
	Ω_3	45.1361	45.1361	45.1361	55.0759	55.0759	55.0759
5	Ω_1	6.9391	7.9790	9.1094	7.1163	8.1648	9.3065
	Ω_2	22.2340	23.5717	25.1345	24.6043	26.0908	27.8311
	Ω_3	47.8600	49.1793	50.7682	58.5679	60.2042	62.1795
10	Ω_1	11.8553	14.1905	16.6439	12.1676	14.5191	16.9959
	Ω_2	29.4809	29.4809	37.4245	32.8996	37.1390	41.7938
	Ω_3	55.0961	59.0961	64.2301	67.8847	73.2615	79.3845
15	Ω_1	17.0078	20.6152	24.3667	17.4498	21.0838	24.8719
	Ω_2	38.5013	44.7447	51.3531	43.2329	50.2622	57.7703
	Ω_3	65.0693	72.6549	80.8113	80.8610	90.5387	101.1210

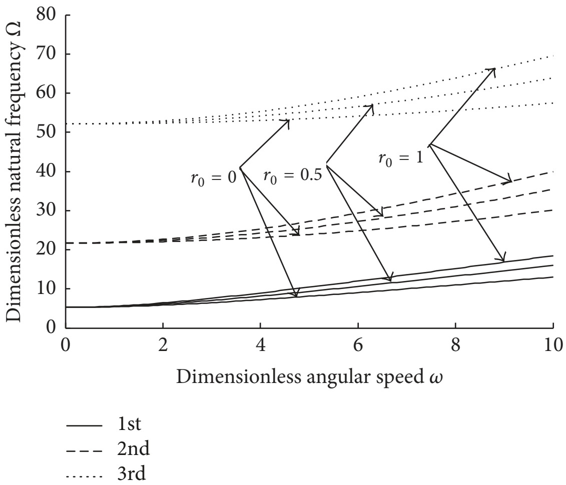

FIGURE 10: The first three-order dimensionless natural frequencies with dimensionless angular speed of the hub for different $r_0 = 0, 0.5, 1$ at $\beta = 0.3$.

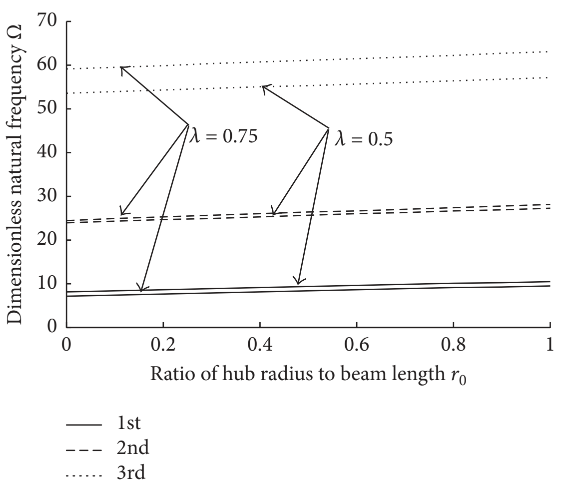

FIGURE 11: The first three-order dimensionless natural frequencies with ratios of hub radius to beam length for $\lambda = 0.5, 0.75$ at $\omega = 5$, $r = 1/30$, and $\beta = 0.3$.

depicted. The main results of this study are summarized as follows.

When the rotating angular speed is constant, in the case of the given ratios of the hub radius to beam length, the slenderness ratio, and the taper ratio of cross-section, the first three-order dimensionless natural frequencies of rotating tapered solid and hollow beams monotonically ascend as the hub dimensionless angular speed increases. For a rotating tapered hollow beam at a constant angular speed, the first-order dimensionless natural frequency of the system is reduced slightly with the increase of the taper ratio of cross-section, the values of the second- and the third-order dimensionless natural frequencies of the system are increased; for different taper ratio of the cross-section and slenderness ratios, with the increase of ratios of hub radius to beam length, the first three-order dimensionless natural frequencies of system almost linearly increase, and the influence of the slenderness

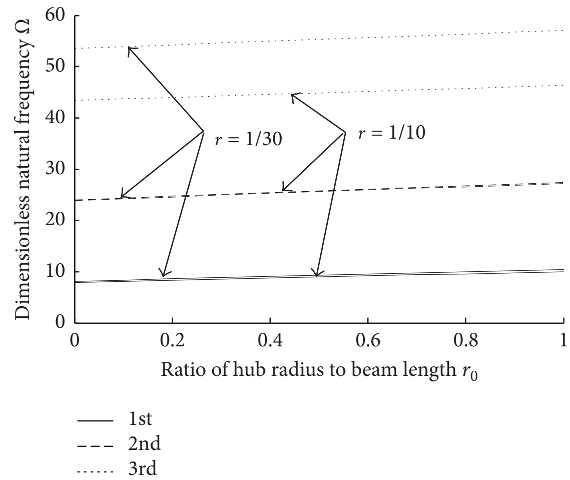

FIGURE 12: The first three-order dimensionless natural frequencies with ratios of hub radius to beam length for $r = 1/30, 1/10$ at $\omega = 5$, $\lambda = 0.5$, and $\beta = 0.3$.

ratio on the third-order natural frequency of the system is more obvious than that of the first order and the second order.

Conflicts of Interest

The authors declare that there are no conflicts of interest regarding the publication of this paper.

Acknowledgments

The authors are grateful for the support from the National Natural Science Foundation of China (Grant no. 11472211).

References

[1] D. Adair and M. Jaeger, "Simulation of tapered rotating beams with centrifugal stiffening using the Adomian decomposition method," *Applied Mathematical Modelling*, vol. 40, no. 4, pp. 3230–3241, 2016.

[2] H. H. Yoo and S. H. Shin, "Vibration analysis of rotating cantilever beams," *Journal of Sound and Vibration*, vol. 212, no. 5, pp. 807–828, 1998.

[3] M. H. Tsai, W. Y. Lin, Y. C. Zhou, and K. M. Hsiao, "Investigation on steady state deformation and free vibration of a rotating inclined Euler beam," *International Journal of Mechanical Sciences*, vol. 53, no. 12, pp. 1050–1068, 2011.

[4] A. S. Vinod Kumar and R. Ganguli, "Violin string shape functions for finite element analysis of rotating Timoshenko beams," *Finite Elements in Analysis and Design*, vol. 47, no. 9, pp. 1091–1103, 2011.

[5] T. Aksencer and M. Aydogdu, "Flapwise vibration of rotating composite beams," *Composite Structures*, vol. 134, pp. 672–679, 2015.

[6] L. Li, W. D. Zhu, D. G. Zhang, and C. F. Du, "A new dynamic model of a planar rotating hub-beam system based on a description using the slope angle and stretch strain of the beam," *Journal of Sound and Vibration*, vol. 345, pp. 214–232, 2015.

[7] J. W. Lee and J. Y. Lee, "In-plane bending vibration analysis of a rotating beam with multiple edge cracks by using the transfer matrix method," *Meccanica*, vol. 52, no. 4-5, pp. 1143–1157, 2017.

[8] J. B. Gunda and R. Ganguli, "New rational interpolation functions for finite element analysis of rotating beams," *International Journal of Mechanical Sciences*, vol. 50, no. 3, pp. 578–588, 2008.

[9] Y. Cheng, Z. Yu, X. Wu, and Y. Yuan, "Vibration analysis of a cracked rotating tapered beam using the *p*-version finite element method," *Finite Elements in Analysis and Design*, vol. 47, no. 7, pp. 825–834, 2011.

[10] G. Bulut, "Effect of taper ratio on parametric stability of a rotating tapered beam," *European Journal of Mechanics - A/Solids*, vol. 37, pp. 344–350, 2013.

[11] J. R. Banerjee and D. R. Jackson, "Free vibration of a rotating tapered Rayleigh beam: a dynamic stiffness method of solution," *Computers & Structures*, vol. 124, pp. 11–20, 2013.

[12] K. Sarkar and R. Ganguli, "Modal tailoring and closed-form solutions for rotating non-uniform Euler-Bernoulli beams," *International Journal of Mechanical Sciences*, vol. 88, pp. 208–220, 2014.

[13] K. Sarkar and R. Ganguli, "Analytical test functions for free vibration analysis of rotating non-homogeneous Timoshenko beams," *Meccanica*, vol. 49, no. 6, pp. 1469–1477, 2014.

[14] A.-Y. Tang, X.-F. Li, J.-X. Wu, and K. Y. Lee, "Flapwise bending vibration of rotating tapered Rayleigh cantilever beams," *Journal of Constructional Steel Research*, vol. 112, pp. 1–9, 2015.

[15] L. Li and D. Zhang, "Dynamic analysis of rotating axially FG tapered beams based on a new rigid-flexible coupled dynamic model using the B-spline method," *Composite Structures*, vol. 124, pp. 357–367, 2015.

[16] Y. Huo and Z. Wang, "Dynamic analysis of a rotating double-tapered cantilever Timoshenko beam," *Archive of Applied Mechanics*, vol. 86, no. 6, pp. 1147–1161, 2015.

[17] V. Panchore, R. Ganguli, and S. N. Omkar, "Meshless local Petrov-Galerkin method for rotating Euler-Bernoulli beam," *CMES: Computer Modeling in Engineering & Sciences*, vol. 104, no. 5, pp. 353–373, 2015.

[18] V. Panchore, R. Ganguli, and S. N. Omkar, "Meshless local Petrov-Galerkin method for rotating Timoshenko beam: a locking-free shape function formulation," *CMES: Computer Modeling in Engineering & Sciences*, vol. 108, no. 4, pp. 215–237, 2015.

[19] M. Ghafarian and A. Ariaei, "Free vibration analysis of a system of elastically interconnected rotating tapered Timoshenko beams using differential transform method," *International Journal of Mechanical Sciences*, vol. 107, pp. 93–109, 2016.

[20] E. Ghafari and J. Rezaeepazhand, "Vibration analysis of rotating composite beams using polynomial based dimensional reduction method," *International Journal of Mechanical Sciences*, vol. 115-116, pp. 93–104, 2016.

[21] V. Panchore and R. Ganguli, "Quadratic B-spline finite element method for a rotating non-uniform Rayleigh beam," *Structural Engineering and Mechanics*, vol. 61, no. 6, pp. 765–773, 2017.

[22] L. Li, D. G. Zhang, and W. D. Zhu, "Free vibration analysis of a rotating hub-functionally graded material beam system with the dynamic stiffening effect," *Journal of Sound and Vibration*, vol. 333, no. 5, pp. 1526–1541, 2014.

[23] G. Zhao and Z. Wu, "Coupling vibration analysis of rotating three-dimensional cantilever beam," *Computers & Structures*, vol. 179, pp. 64–74, 2017.

[24] L. Li and D. G. Zhang, "Free vibration analysis of rotating functionally graded rectangular plates," *Composite Structures*, vol. 136, no. 2, pp. 493–504, 2016.

[25] H. Zafarmand and M. Kadkhodayan, "Nonlinear analysis of functionally graded nanocomposite rotating thick disks with variable thickness reinforced with carbon nanotubes," *Aerospace Science and Technology*, vol. 41, pp. 47–54, 2015.

[26] T. Dai and H.-L. Dai, "Thermo-elastic analysis of a functionally graded rotating hollow circular disk with variable thickness and angular speed," *Applied Mathematical Modelling*, vol. 40, no. 17-18, pp. 7689–7707, 2016.

[27] Y. F. Zhou and Z. M. Wang, "Application of the differential quadrature method to free vibration of viscoelastic thin plate with linear thickness variation," *Meccanica*, vol. 49, no. 12, pp. 2817–2828, 2014.

[28] Y. F. Zhou and Z. M. Wang, "Vibrations of axially moving viscoelastic plate with parabolically varying thickness," *Journal of Sound and Vibration*, vol. 316, no. 1–5, pp. 198–210, 2008.

[29] L. Meirovitch, *Elements of Vibration Analysis*, McGraw-Hill, Singapore, 1986.